Available online at www.sciencedirect.com
SCIENCE DIRECT®
Journal of Power Sources 118 (2003) 79–85
JOURNAL OF POWER SOURCES
www.elsevier.com/locate/jpowsour

Computer methods for performance prediction in fuel cells

S.B. Beale[a,*], Y. Lin[a], S.V. Zhubrin[b], W. Dong[a,1]

[a]National Research Council, Montreal Road Ottawa, Ottawa, Ont., Canada K1A 0R6
[b]Concentration Heat and Momentum Ltd., 40 High Street, Wimbledon Village, London SW19 5AU, UK

Abstract

Several transport models for fuel cells have been developed. The models are compared and tested for single fuel cells and multi-cell stacks of planar solid-oxide fuel cells, the three main approaches considered are (a) a detailed numerical model (DNM) of flow, heat and mass transfer and electrochemistry, (b) a flow-based methodology based on a distributed resistance analogy (DRA), and (c) a presumed-flow methodology (PFM). The results from each of the above approaches are compared in detail, and merits and drawbacks discussed. It is shown that, under certain circumstances, the simpler approaches have the potential to supplant or complement the direct numerical method in the analysis of fuel cells.

Keywords: Fuel cells; Transport phenomena; Computational fluid dynamics; Heat transfer; Electrochemistry

1. Introduction

High power generation and heat recovery efficiency with low pollution rate make fuel cells [1] potential useful energy conversion systems. Initial modelling efforts have been focused on planar solid oxide fuel cells (SOFCs). Experimental data are scarce and for this reason substantial effort is being devoted to developing numerical analysis tools capable of performing calculations on transport and electrochemical phenomena within the passages of fuel cells.

Since the first SOFC computations, Vayenas and Hegedus [2], the detail of the mathematical modeling has increased. Numerical simulations have been conducted at the electrode, cell, and stack levels. Modelling at the electrode level aims at building better electrodes through study of microscopic processes, while modelling at the stack level aims at optimizing the design, by considering alternatives and determining operational strategies. Chemical reactions (shift reactions and internal reforming), electrical potential distribution, and porous-media flow are all issues to be addressed.

Fiard and Herbin [3], Ferguson [4], Herbin et al. [5], and Bernier et al. [6] developed a detailed three-dimensional (3D) SOFC model with governing equations for mass, heat and electrical current for both solid and gas-channel flows. Numerical schemes for the boundary condition at the interfaces between the electrolyte and electrodes are given. The 3D model was applied to planar stack simulations. Karoliussen and Nisanciouglu [7], Achenbach [8], Bessette and Wepfer [9], and Bernier et al. [6] took into account the reforming and shift reactions in their respective models. In addition, Ahmed et al. [10], Sira and Ostenstad [11], Achenbach [8], Bessette and Wepfer [9], Costamagna and Honegger [12], Chan et al. [13], Dong et al. [14] and Beale et al. [15,16] applied their models to heat and mass transfer in SOFCs.

The complexity of the SOFC problem requires the use of large fast computers to tessellate the geometry into a large number of mesh points, and solve the coupled partial differential equations describing the transport phenomena. The theoretical framework for stack modeling based on simplified numerical methods, so that numerical simulation become tractable on personal computers, was introduced by various authors, Achenbach [8], Bernier et al. [6], Beale et al. [15]. Both single cells and stacks of fuel cells are considered in the present work. Fig. 1 is a schematic of a stack considered in this study.

2. Mathematical formulation

2.1. Detailed numerical model (DNM)

For single cells and small stacks it is possible to discretize the entire domain and solve the governing equations directly.

* Corresponding author. Tel.: +1-613-993-3487; fax: +1-613-941-1571.
E-mail address: steven.beale@nrc.ca (S.B. Beale).
[1] Present address: Global Thermoelectric Inc., 4908—52nd Street, S.E. Calgary, Alta., Canada T2B 3R2.

0378-7753/03/$ – see front matter.
doi:10.1016/S0378-7753(03)00065-X

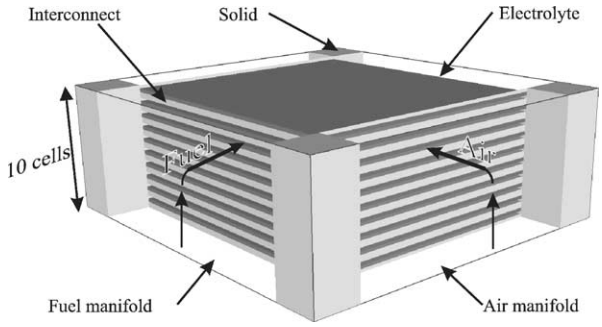

Fig. 1. A 10-cell stack considered in this study.

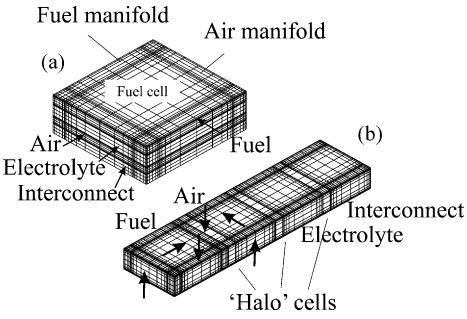

Fig. 2. Computational mesh for (a) DNM, (b) DRA.

This is referred to below as a detailed numerical model (DNM). The equations to be considered are the usual transport equations, namely

$$\frac{\partial(\rho r\phi)}{\partial t} + \mathrm{div}(\rho\vec{u}\phi) = \mathrm{div}\,\Gamma\,\mathrm{grad}\,\phi + S \tag{1}$$

where ϕ takes the value 1 (continuity), $\vec{u}$ (momentum), y_i (mass fraction) and h (enthalpy), and Γ and S are exchange coefficients and source terms, respectively. Reynolds numbers for both fuel and air are small, and a turbulence model was not therefore invoked. Solid and fluid physical properties were similar to those given in Beale et al. [16].

At the anode surface, electrochemical oxidation takes place as

$$H_2 + O^{2-} \rightarrow H_2O + 2e^- \tag{2}$$

$$CO + O^{2-} \rightarrow CO_2 + 2e^- \tag{3}$$

At the cathode surface, reduction takes place

$$O_2 + 4e^- \rightarrow 2O^{2-} \tag{4}$$

The surface rates, J, for H_2, H_2O and O_2 are required to compute mass and species source terms. These can be related to local current density, i, by Faraday's law

$$J = -\frac{M}{1000}\frac{i}{vF} \tag{5}$$

where M is molecular weight, v the valence, and F the Faraday's constant. The cell voltage, V, can be computed as

$$V = E - iR_i - \eta_a - \eta_c = E - iR_i' \tag{6}$$

where η_a and η_c are anodic and cathodic overpotentials. R_i ($\Omega\,m^2$) is the local Ohmic resistance, R_i' ($\Omega\,m^2$) can be regarded as a locally 'lumped internal resistance' of the cell. E is the Nernst potential;

$$E = E^0 + \frac{RT}{2F}\ln\left(\frac{y_{H_2}y_{O_2}^{0.5}}{y_{H_2O}}\right) + \frac{RT}{4F}\ln P_a \tag{7}$$

where y_i are mole fractions, and P_a the air pressure. For the results presented in this paper, a fourth-order least-squares polynomial [14] fitted to experimental data in the range 550–1200 °C, was used to compute the Ohmic resistance and electrolyte overpotentials in Eq. (6), though latterly a Butler–Volmer equation is now being used compute the overpotentials in Eq. (6), explicitly.

The local heat source due to the electrothermal effect of Ohmic resistance and overpotentials can be expressed as

$$\dot{q}_e = \frac{i(E-V)}{L_{cell}} \tag{8}$$

where L_{cell} is the thickness of the cell sheet.

A finite volume method is used to solve the partial differential equations subject to appropriate boundary conditions. The geometry is, such that a Cartesian mesh, passing through both solid and fluid zones, was conveniently employed. Fig. 2a shows a computational mesh used to perform calculations using a DNM. The main components of the cell are fuel channels, electrolyte and electrodes, air channels, and interconnects. Fuel and air are in cross-flow. Two designs were considered: (a) with both the fuel and air channels in the form of flat rectangular ducts; (b) with numerous individual air channels and a single rectangular fuel channel. Overall dimensions, boundary conditions, etc. are the same in both cases. Current density, temperature, power density, lumped resistance, and fuel utilization were all computed.

The calculation proceeds as follows: (1) initial values are assumed for transport properties and cell voltage V. (2) The main calculation procedure is commenced and heat and mass source terms computed. The transport equations, Eq. (1), are solved. (3) The Nernst potential and internal resistance are then computed, and the local current density obtained. Steps (2) and (3) are repeated until sufficient convergence is obtained. Either the cell voltage, V, or the current, I, (or equivalently mean current density, $\bar{i}$) must be prescribed. Earlier work by our group was for the case of prescribed cell voltage, V. Our preference for prescribing current density here is driven by the need to ensure charge conservation from cell-to-cell within a stack. For this case, the cell voltage is adjusted iteratively until the correct value of $\bar{i}$ is obtained. This is quite straightforward.

The DNM was used to calculate performance in both single-cells and in the manifolds and passages of stacks of cells. Two distinct commercial computer codes, Phoenics and Fluent, were employed for this class of analysis. In both

cases the details of the electrochemical reactions were written in Fortran or C and called during run-time by the flow solver.

2.2. Distributed resistance analogy (DRA) and presumed flow methods (PFMs)

Because detailed numerical simulations require very large computational resources, an alternative methodology was devised for stack modeling. The method is a modified version of the DRA of Patankar and Spalding [17]. The flow of both working fluids with the associated coupled heat/mass transfer is computed using local volume-averaging so that,

$$\frac{\partial(r\rho)_i}{\partial t} + \mathrm{div}(r\rho\vec{u})_i = r_i S_i \tag{9}$$

$$\frac{\partial(\rho r\vec{u})_i}{\partial t} + \mathrm{div}(\rho r\vec{u};\vec{u})_i = -r_i \,\mathrm{grad}\, p_i + \mathrm{div}(r\mu \,\mathrm{grad}\,\vec{u})_i + r_i S_i \tag{10}$$

$$\frac{\partial(\rho r\phi)}{\partial t} + \mathrm{div}(r\rho\phi)_i = \mathrm{div}(r\Gamma \,\mathrm{grad}\,\phi)_i + r_i S_i \tag{11}$$

where i is the air, fuel, electrolyte (including the electrodes), interconnect materials, as appropriate. Source terms $S_i = (Fr\vec{u})_i$ are introduced into Eq. (10); F is referred to as α 'distributed resistance'. For heat transfer, inter-phase terms having the form $r_i S_i = \sum_j \alpha_{ij}(\phi_j - \phi_i)$ are introduced to account for fluid-to-solid and solid-to-fluid heat transfer. Values of F and α may be obtained from analytical, numerical or experimental analysis. Here analytical expressions for flow and heat transfer in ducts were used, Beale et al. [18].

Continuity and concentration sources and sinks per unit volume account for heterogeneous chemical reactions. State variables may now be considered as being interstitial bulk values. Diffusive terms are eliminated from fluid regions, while convective terms are superfluous in solids. Two velocities and pressures, corresponding to air and fuel, are solved for in each computational cell, and temperatures in all fluid and solid zones. This is implemented with a multiply shared space method, Spalding and Zhubrin [19], Zhubrin [20]. The domain is decomposed into four separate spatial blocks in order to solve for air, fuel, electrolyte, and metallic interconnect materials, as shown in Fig. 2b. Inter-phase source terms are passed back and forth spatially between the four blocks. The computer code Phoenics was used to develop this capability. At present the DRA is only implemented for constant current density.

A presumed flow method (PFM), based on rate equations, represents the simplest possible methodology. The pressure-corrected momentum equations are not solved, but the continuity equations, which assume a simplified ordinary differential form for single-pass cross-flow, account for the production and destruction of chemical species. For heat/mass transfer, inter-fluid transfer terms and Ohmic heat per unit volume in the electrolyte are as prescribed as above. Beale et al. [16] showed that the heat conduction in the highly-conducting interconnect material cannot be neglected, and an iterative solver was therefore used to obtain a numerical solution to the governing system of equations. Although referred to as a 'presumed flow' method the mass flow rates are in fact adjusted to account for the generation/depletion of matter due to electrochemical reactions. A rate equation is used, as above, to compute wall mass fraction from bulk values and hence wall mole fractions for use in the Nernst equation, Eq. (7), and the source terms in the transport equations. A multiply-shared method is not required, since an in-house PFM code was developed in C^{++}, where the spatial discretization is chosen to correspond to the cell materials. The code is capable of modelling single cells and fuel cell stacks, for variable current density, however unlike the DRA method, flow in the manifolds cannot be detailed at present, only that within the passages of the fuel cell.

3. Results

All three classes of code were employed in the study of both single fuel cells and stacks of cells under a variety of operating conditions. The dimensions of the reference geometry are nominally 0.1 m × 0.1 m. Boundary conditions and property values are similar to those given in reference [16]. Detailed comparisons of the models were undertaken for a single cell of known geometry with constant mass source (i.e. current density) and heat source, and also under the more realistic situation where average current (density) is pre-defined, and local current density and resistance computed, iteratively. For a 10-cell stack, a model for variable local current density is used to perform calculations in the absence of manifolds, i.e. presumed uniform flow at fuel and air inlets. Studies were also conducted for full manifold-stack assemblies corresponding to an actual design based on the assumption of constant local current density.

Fig. 3 shows level-lines for temperature obtained from DNM and PFM methods under the 'idealized' conditions of presumed constant mass/heat source corresponding to

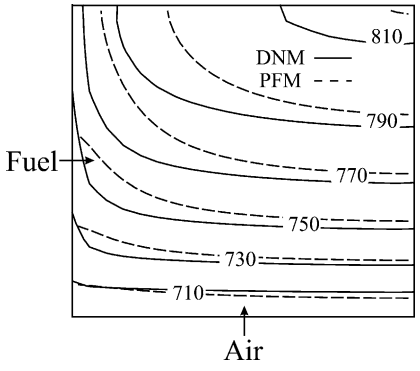

Fig. 3. Cell temperature, T, (°C), constant $i = 4\,000$ A/m^2, $P = 1.5$ W/m^3 (plan view).

$i = 4\,000$ A/m^2, $\dot{q} = 1.5 \times 10^6$ W/m^3. Figs. 4–10 show results for a single cell with variable local current density corresponding to a prescribed mean value. Figs. 4–6 show hydrogen mass fraction, cell temperature, and current density, for $\bar{i} = 4\,000$ A/m^2; the local cell resistance is computed according to reference [14]. Data obtained from DNM and PFM calculations are exhibited. Figs. 7–10 are similar plots of cell temperature, and current density for $\bar{i} = 6\,000$ and $2\,000$ A/m^2 (DNM only). Fig. 11 shows the voltage versus current density characteristic curve, corresponding to H_2 and O_2 utilisation factors of 0.6 and 0.25, respectively.

The results of calculations of the performance of a 10-cell stack are shown in Figs. 12–15. Figs. 12 and 13 show elevation views of temperature in a 10-cell stack, assuming

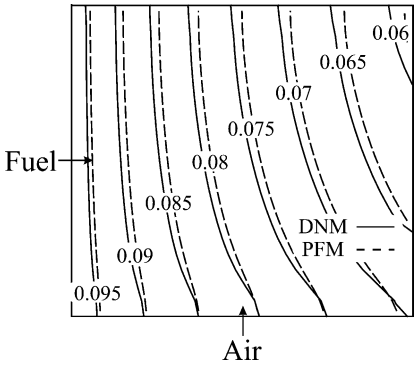

Fig. 4. Mass fraction, H_2, variable current density, $\bar{i} = 4\,000$ A/m^2.

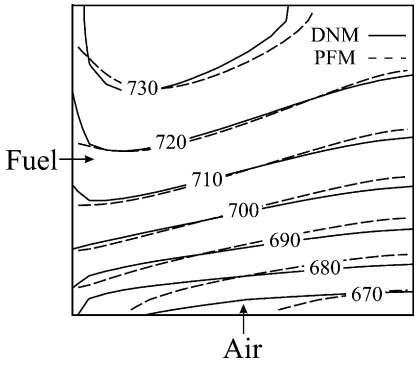

Fig. 5. Temperature, T, (°C), variable current density, $\bar{i} = 4\,000$ A/m^2.

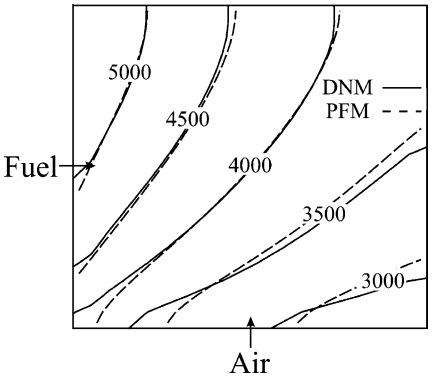

Fig. 6. Current density, i, (A/m^2), $\bar{i} = 4\,000$ A/m^2.

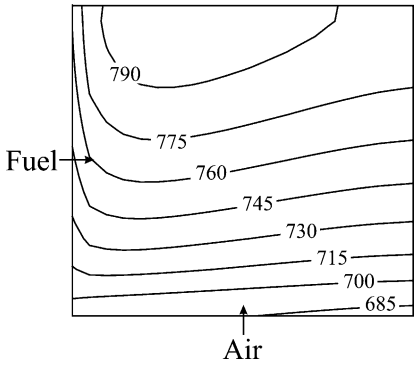

Fig. 7. Temperature, T, (°C), $\bar{i} = 6\,000$ A/m^2.

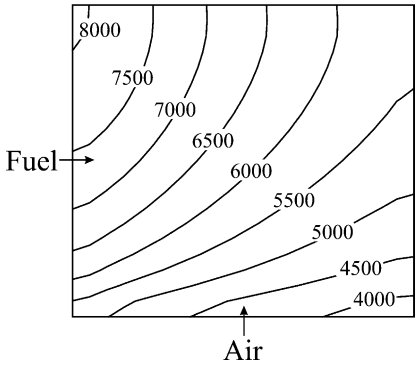

Fig. 8. Current density, i, (A/m^2), $\bar{i} = 6\,000$ A/m^2.

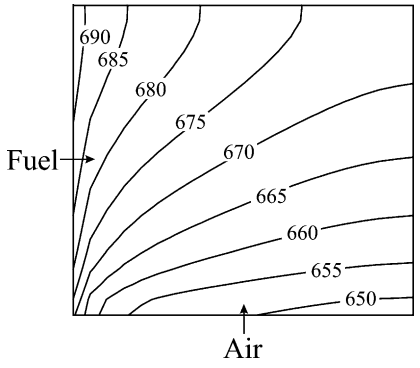

Fig. 9. Temperature, T, (°C), $\bar{i} = 2\,000$ A/m^2.

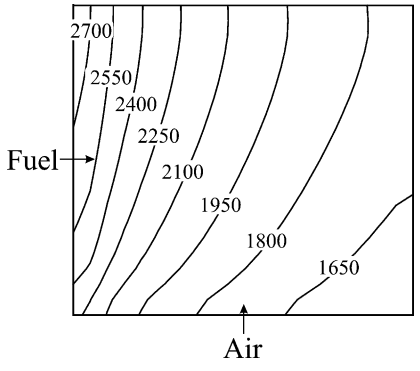

Fig. 10. Current density (A/m^2), $\bar{i} = 2\,000$ A/m^2.

constant $i = 4\,000$ A/m^2, $\dot{q} = 1.5 \times 10^6$ W/m^3 obtained using the DNM and DRA methods. Figs. 14 and 15 are views of the temperature distribution and current density obtained for variable current density corresponding to a mean value of $\bar{i} = 4\,000$ A/m^2. The latter are for a stack with no manifolds.

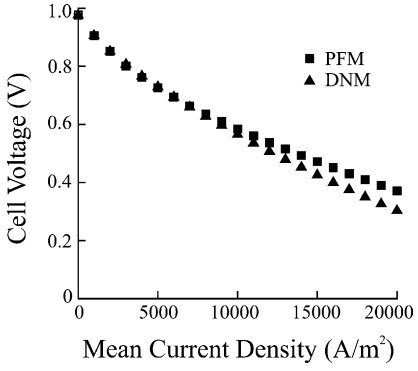

Fig. 11. Cell voltage as a function of mean current density.

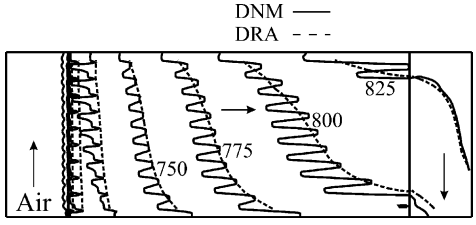

Fig. 12. Temperature, T, (°C), constant $i = 4\,000$ A/m^2, $P = 1.5$ W/m^3. 10-cell stack, adiabatic walls (elevation view).

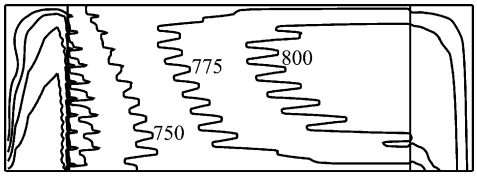

Fig. 13. Temperature, T, (°C), constant $i = 4\,000$ A/m^2, $P = 1.5$ W/m^3. 10-cell stack, constant temperature walls, $T_W = 750$ °C.

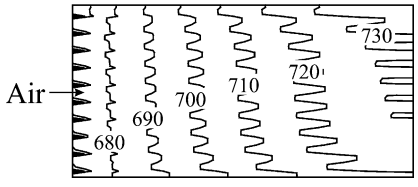

Fig. 14. Stack temperature (°C), $\bar{i} = 4\,000$ A/m^2, DNM.

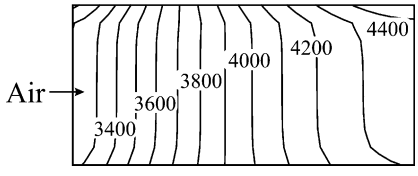

Fig. 15. Current density (A/m^2), $\bar{i} = 4\,000$ A/m^2, PFM.

4. Discussion

Inspection of Fig. 3 reveals that for the 'idealized case' of uniform heating and mass transfer by the electrolyte; the temperature is lowest at the location corresponding to the (bottom–left) air-fuel inlets, and highest at the corresponding outlets (top–right). The bi-linear temperature distribution associated with cross-flow is due to the overall energy balance being dominated by the convection and heat-source terms. Thus, even if the fluid flow and chemical reaction rates are completely uniform, there will be temperature gradients in the fuel cell: one factor tending to smooth and reduce undesirable gradients [16] is the metallic interconnect. Thus for thermal management, a thick, highly-conducting interconnect is desirable. It can be seen from Fig. 3, that there is reasonably good agreement between the data for the DNM and PFM methodologies. The differences are due to the approximate nature in the choice of Nusselt numbers required for the PFM model.

Inspection of Figs. 4–6, for variable local current density and electrical resistance, further reinforce the fact that a reasonable estimate of the thermo-mechanical and electrochemical performance of a fuel cell in cross-flow, can be obtained using a PFM, at a fraction of the computer speed and memory required to perform a detailed computational fluid dynamcs (CFD) based calculation, provided the inlet conditions are uniform. Contours of Nernst potential (not shown) follow those of hydrogen mass fraction, Fig. 4. Because current density, and hence power density, are higher at the top–left corner of Fig. 6, the global temperature maximum shifts to this location. The cell resistance is also a minimum at this point. Non-uniform reaction kinetics will re-distribute the temperature field, but may not necessarily result in higher temperature gradients (NB: the results of Figs. 3 and 5 are not quantitively comparable, due to differences in cell resistance). Reference [18] discusses how uniform flow conditions may be achieved. At $\bar{i} = 4\,000$ A/m^2, the cell voltage computed from the PFM is within 0.5% of that obtained with the DNM, with a lower cell voltage predicted by the DNM, and corresponding heat source in Eq. (8), thus affecting the temperature distribution in Fig. 3, though agreement between DNM and PFM is still within 5 °C.

Detailed calculations were also performed for average current densities of 2 000 and 6 000 A/m^2. Agreement in terms of local current density, between the PFM and DNM distribution (not shown) is generally good. Comparison of the results for $\bar{i} = 2\,000$, 4 000, 6 000 reveals the temperature distribution to be a strong function of the load, while the current density is relatively independent, indicating that low fuel and air utilizations are achieved. At $\bar{i} = 2\,000$ A/m^2, the temperature profile resembles that of a simple cross-flow heat exchanger, due to the difference in temperature between the two working fluids being large compared to the overall temperature rise due to the electrical heating.

At $\bar{i} = 6\,000$ A/m^2, the converse is true. The current density contours, as shown in Figs. 6, 8, 10 are relatively similar over this range of loads. For the DNM calculations, very good agreement was obtained when using two different CFD codes; Phoenics and Fluent.

Inspection of the results of the voltage current-density distribution curve, Fig. 11, also reveal that very good agreement is obtained between the DNM and PFM methods, at least for values of current density up to $\bar{i} = 10\,000$ A/m^2. At higher values of $\bar{i}$ some significant error becomes apparent, due to the assumption of constant Nusselt/Sherwood number being invalid at these high mass transfer rates.

Figs. 12 and 13 show temperature distributions for a 10-cell stack model at constant $i = 4\,000$ A/m^2 under adiabatic and isothermal boundary conditions, respectively. The results shown in Fig. 12 are for presumed adiabatic walls, corresponding to a well-insulated stack. Excellent agreement is observed between the results of the DNM and DRA calculations. The 'zig-zag' pattern exhibited by the DNM is absent for the DRA because a multi-space approach is employed, and only the air-space temperature is displayed, whereas for the DNM, the temperatures in the air, fuel, electrolyte and interconnect zones vary on a cell-by-cell basis. The arising temperature field is three-dimensional (3D) [16] even though the fluid flow and current density distributions are uniform. This is due to the fact that the fuel and air streams are at different temperatures, and that the order of the materials is repeated in the vertical direction. Thus the common assumption that a single-cell model with periodic boundary conditions may be used to predict stack performance is erroneous. In the current DRA implementation, the vertical-k-direction influence was correctly accounted-for by meshing the geometry so that computational cells corresponded to fuel cells, and prescribing the electrode-fuel (ef) pair of inter-phase source terms in Eq. (11) so that these were across $n-1$ neighbour values $\alpha_{\mathrm{ef}}(\phi_{\mathrm{e},k+1} - \phi_{\mathrm{f},k})$ and $\alpha_{\mathrm{ef}}(\phi_{\mathrm{f},k-1} - \phi_{\mathrm{e},k})$, not n in-cell values $\alpha_{\mathrm{ef}}(\phi_{\mathrm{e},k} - \phi_{\mathrm{f},k})$, $k = 1, 2, 3, \ldots, n$, as were all other terms (electrode-air, air-interconnect, fuel-interconnect, etc.). With this important modification, it can be seen that the DRA approach generates the 3D results obtained with the detailed CFD simulation at a fraction of the computational cost. Any volume-averaging or 'porous-media' technique which does not account for the effects due to the ordering of the streams, will incorrectly generate constant temperature profiles in the vertical direction.

Fig. 13 shows the results for the corresponding constant wall temperature case, corresponding to the limiting case of an uninsulated stack immersed inside an oven at 750 °C. The reader will note that although the isotherms at the wall in Fig. 13 are parallel rather than normal to the wall, similar temperature distributions are observed in the interior of the fuel cell as for the adiabatic case, Fig. 12. This suggests that temperature control may be a matter for concern for the fuel cell designer employing prototypes in experimental test rigs, where the interior temperatures may exceed surface values. Figs. 14 and 15 show the contours of temperature and current density in a 10-cell stack obtained at variable current density, corresponding to $\bar{i} = 4\,000$ A/m^2. The secondary temperature effects are less pronounced than in Fig. 13, because, the power consumption is lower; however, they are readily apparent. The reader will also note that predicted local current density displays 3D effects, due to the sensitivity of cell resistance to local temperature.

5. Conclusions

Calculations were performed on single and 10-cell stacks of SOFC fuel cells using three distinct approaches referred to as the PFM, DRA and DNM. Both constant heat and current density, and variable local current density, corresponding to known average values of $\bar{i}$, were considered under adiabatic and isothermal wall conditions. For single cells, all of these methods can be reliably used to perform calculations in planar SOFCs with the DNM being the most accurate since it does not require prescription of overall heat and mass transfer coefficients. For large stacks of fuel cells, however the DNM requires very large computational meshes, resulting in large data sets and compute times. Under these circumstances, if it is known that the flow is fully-developed and uniform, a PFM should be considered as an alternative or complementary simulation tool at a fraction of the compute cost. The DRA represents a compromise between cost and performance, and can be used in situations where the flow and pressure distributions in the stack are not necessarily uniform. It is important that when 'local volume-averaging' techniques are employed, secondary transport phenomena are not obscured.

The key difference between the PFM/DRA and the DNM program is in the specification of overall heat/mass coefficients. Any errors in these values will impact the Nernst equation and the local cell resistance. The results presented in this paper are relatively preliminary, and we anticipate further reconciliation between the different modelling techniques as experience is gained. It is to be noted that many alternatives are possible; the DRA could be replaced by a code whereby detailed flow models based on CFD are obtained in necessary zones, such as manifolds, but that a PFM model be adopted in the stack where additional storage is provided-for auxiliary variables, such as current density and potential, which are not required elsewhere.

6. Future work

A semi-empirical resistance model, which combines the Ohmic and overpotential terms was used in this paper, owing to the sparse experimental data available for the particular

design under consideration. This has now been supplanted with a Butler–Volmer equation for anodic and cathodic overpotential in most of the codes, and the latter will be adopted from now on. To further improve the correlation between the PFM, DRA, and DNMs, additional effort is required when prescribing mass transfer coefficients, and use of Stefan–Maxwell equations for multi-species mass diffusion coefficients, in place of the simple Fickean analysis developed here, is a worthwhile undertaking.

Many workers are now modelling the electrical potential and current collection associated with porous-media diffusion and chemical reactions in a fully-coupled manner. The simplified model used here, where the electrolyte includes the electrodes is considered appropriate for thin planar geometries, but may not be valid for other, more complex fuel-cell designs. Under these circumstances detailed numerical analysis may subsequently be used to prescribe electrical and thermal shape factors, needed to compute heat/mass transfer coefficients for the rate equations. Moreover the details of the chemical reactions have been kept simple; for a first analysis important phenomena such as internal reforming have been excluded in the interest of simplicity. For the same reasons radiation heat transfer was also neglected. Future work will include these.

The success of the PFM and the DRA are due, in part to the ease of constructing models for single-pass cross-flow. For multi-pass flow and/or where the flow channels are of arbitrary location and direction (i.e. not necessarily oriented along well-defined geometric lines), the scientific principles remain the same, but the problem of engineering codes under these circumstance is a challenge. In modifying the DRA to correctly predict 3D phenomena, it was necessary for the computational mesh to conform to the boundaries of the fuel cells in the stack, so that neighbour values be correctly prescribed. Some further research work is required to allow for the DRA to be employed with aribitrary non-body-fitting meshes.

The need for reliable experimental data is readily apparent, and while gathering such data can be substantially more time-consuming than constructing models and performing numerical calculations, the availability of such data are critical for the evaluation and improvement of existing numerical models. Although most of the work to-date has been concerned with SOFCs, much of the modelling expertise can readily be modified for application to other fuel cells, such as proton exchange membrane fuel cells. This avenue is actively being pursued by a majority of the authors.

Acknowledgements

Financial support for this work was provided by the Fuel Cells Program of the National Research Council. Ron Jerome provides technical support for our research group. We would also like to thank Global Thermoelectric Inc., for their technical and financial support in the early stages of this research program.

References

[1] A.J. Appleby, F.R. Foulkes, Fuel Cell Handbook, Van Nostrand, New York, 1989.
[2] C.G. Vayenas, L.L. Hegedus, Ind. Eng. Chem. Fundam. 24 (1985) 316–324.
[3] J.M. Fiard, R. Herbin, Comput. Methods Appl. Mech. Eng. 115 (1994) 315–338.
[4] J.R. Ferguson, in: Proceedings of the Second International Symposium on Solid Oxide Fuel Cells, Athens, Greece, 1991, pp. 273–280.
[5] R. Herbin, J.M. Giard, J.R. Ferguson, in: Proceedings of the First European Solid Oxide Fuel Cell Forum l, Lucerne, Switzerland, 1994.
[6] M. Bernier, J.R. Ferguson, R. Herbin, in: Proceedings of the Third European Solid Oxide Fuel Cell Forum, Nantes, France, 1998, pp. 483–495.
[7] H. Karoliussen, K. Nisanciouglu, in: Proceedings of the Third International Symposium on Solid Oxide Fuel Cells, Honolulu, Hawaii, USA, 16–21 May 1993, pp. 868–877.
[8] E. Achenbach, J. Power Sources 49 (1994) 338–348.
[9] N.F. Bessette, W.J. Wepfer, Chem. Eng. Commun. 147 (1996) 1–15.
[10] S. Ahmed, C. McPheeters, R. Kumar, J. Electrochem. Soc. 138 (1991) 2712–2718.
[11] T. Sira, M. Ostenstad, in: Proceedings of the Third International Symposium on Solid Oxide Fuel Cells, Honolulu, Hawaii, USA, 16–21 May 1993, pp. 851–860.
[12] P. Costamagna, K. Honegger, J. Electrochem. Soc. 145 (11) (1998) 3994–4007.
[13] S.H. Chan, K.A. Khor, Z.T. Xia, J. Power Sources 93 (2001) 130–140.
[14] W. Dong, S.B. Beale, R.J. Boersma, in: Proceedings of the CFD Society of Canada, 2001, pp. 382–387.
[15] S.B. Beale, W. Dong, S.V. Zhubrin, R.J. Boersma, in: Proceedings of the ASME IMECE2001/PID-25615, New York, 11–16 November 2001.
[16] S.B. Beale, S.V. Zhubrin, W. Dong, in: Proceedings of the 12th Conference on International Heat Transfer, Grenoble, France, 2002, pp. 865–870.
[17] S.V. Patankar, D.B. Spalding, TR EF/TN/A/48, Imperial College, London, 1972.
[18] S.B. Beale, A. Ginolin, R. Jerome, M. Perry, D. Ghosh, PHOENICS J. Comput. Fluid Dyn. 13 (3) (2000) 287–295.
[19] D.B. Spalding, S.V. Zhubrin, in: Proceedings of the Eighth International PHOENICS User Conference, Luxembourg, 2000.
[20] S.V. Zhubrin, in: Proceedings of the Seventh International PHOENICS User Conference, Seville, Spain, 1997.